Optimizing Tracking Loops for UWB Monocycles

Chee-Cheon Chui and Robert A. Scholtz[1]
Communication Science Institute
University of Southern California
Los Angeles, CA 90089-2565

Abstract - **This paper explores a correlation timing detector for tracking of Ultra-Wide-Band (UWB) monocycle signals. We seek to examine the optimal relationship between the received and reference UWB monocycle waveforms considering timing jitter and the ability to acquire lock. We modeled the received UWB monocycle waveform as the n^{th} order derivative of the Gaussian function. We are able to obtain a good fit using the UWB model with n=4 to both UWB impulses measured in an anechoic chamber and UWB impulses obtained in an indoor office environment. The UWB monocycle model, though an idealized representation, allows us to derive a closed form expression for the slope of the characteristic function of the TLL when both the received and reference monocycle are of arbitrary and different orders n and m. Using this compact formula, we can analyze the timing jitter of the error-tracking TLL in an additive white Gaussian noise (AWGN) channel. Computer simulation is also used to examine the dynamics of the tracking process when the loop is second order. Notably the phase plane plot is examined that gives us an indication of the ability of the TLL to acquire lock. The analysis allows us to make informed choices of the order of the monocycle waveform considering trades-off between timing error variance due to AWGN in the channel and the ability of the TLL to acquire lock. We conclude this paper by discussing a possible automatic gain control (AGC) scheme, whose main purpose is to remove the dependence of the TLL on variations in input signal amplitude.**

I. INTRODUCTION

There has been widespread interest in the communication community to utilize UWB impulses for wireless communication, imaging and ranging. Such UWB impulses do not rely on a sinusoidal carrier for transmission.

Extensive research was done since the 1960s on Phased-Locked Loops (PLL) and baseband code tracking loops. The PLL is used in wireless communications systems in which information to be transmitted is superimposed on a sinusoidal carrier. Further differences between baseband code and UWB monocycle tracking include the low duty cycle and the significantly larger bandwidth in the latter. Consequently the effect of pulse shaping by the antenna cannot be ignored, and it is no longer adequate to model the received waveform simply as rectangular or raised cosine pulses as commonly done in narrowband signals. This motivates us, drawing on developed PLL, delay locked loop and code tracking loop theories detailed in [8][11][12], to devise and investigate equivalent error tracking PLL/Time-Locked-Loop (TLL) for tracking of UWB impulses. This paper is devoted to examining the suitability of our proposed timing detector and analyzing its performance when utilized for tracking UWB monocycle in a TLL for a AWGN channel.

The 2nd order derivative Gaussian pulse has been widely utilized by many authors to evaluate the performance of their UWB systems. This paper presents a general formula for an n^{th} order derivative Gaussian monocycle and uses it to model the received monocycle waveform. We treat the order n as a design parameter and examine its choice in the context of tracking of UWB impulses. We show here that the appropriate choice of n will indeed have impact on the performance of an UWB impulse transceiver.

II. TIME-LOCKED LOOP

We consider a received signal given by

$$y(t) = A_s \sum_k q(t - k\Omega - \xi) + n(t)\,, \qquad (1)$$

where we have assumed the communication channel is corrupted by AWGN noise $n(t)$ that has zero mean and one-sided power spectral density N_o. The received UWB monocycle waveform with unit energy is denoted as $q(t)$, the unknown time delay is ξ and the pulse repetition period Ω. The energy of each received monocycle in the absence of noise is A_s^2. The reference signal generated at the receiver is

$$s(t) = A_r \sum_k r(t - k(\Omega + \theta) - \hat{\xi})\,, \qquad (2)$$

where $r(t)$ represents the reference signal waveform with unit energy. The energy per monocycle of the reference signal is A_r^2. Here θ is used to represent the difference in pulse repetition period between the transmitter and receiver in units of seconds, and $\hat{\xi}$ is the estimate of ξ in (1). We define the following timing processes:

$$\begin{cases} T_k = k\Omega + \xi \\ \hat{T}_k = k\Omega + k\theta + \hat{\xi} \end{cases}. \qquad (3)$$

The timing offset between the transmitter and receiver when receiving the k^{th} monocycle is:

$$\varepsilon_k = T_k - \hat{T}_k\,. \qquad (4)$$

Using terminology commonly understood in tracking of sinusoidal signals, $\xi - \hat{\xi}$ and θ are analogous to the 'phase step' and 'frequency step' respectively.

[1]This work was supported in part by a MURI Project under Contract DAAD 19-01-1-0477 from the US Army Research Office. Chee-Cheon Chui's postgraduate study in USC is supported by DSO National Laboratories, Singapore.

To track the received UWB monocycles, we employ a time-locked loop which has a structure similar to conventional baseband timing tracking loops and code tracking loops. The TLL to be described here has the general structure shown in Fig. 1. The reference signal at the receiver is an odd function if the received monocycle is modeled as an even function and vice versa. If *q(t)* is even, possible candidates for *r(t)* are the Hilbert transform of *q(t)*, the odd-order derivative of the Gaussian function or a rectangular function with opposite signs in opposite sides of $t = 0$.

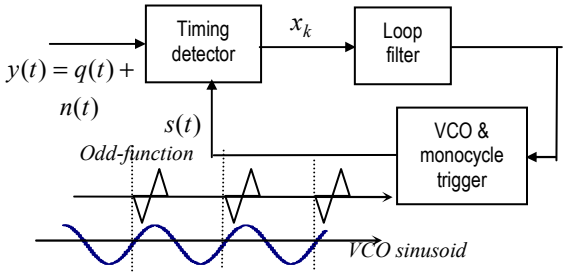

Figure 1: General structure of the TLL for tracking of UWB impulses. It is assumed that the UWB monocycles, triggered by the positive-going zero-crossings of a sinusoid oscillator, serve as timing for the system.

The working of the correlation timing detector is shown in Fig. 2. It correlates the received UWB impulses with the reference signal generated at and timed by the local voltage control oscillator (VCO) of the receiver. The timing detector operates nominally at symbol/pulse repetition rate, i.e., the timing error is computed, and the control signal to the VCO is updated only once per pulse repetition period (or per received UWB impulse). The output of the timing detector will be a signal proportional in magnitude and of the same sign (for positive loop gain) as the timing difference between the received signal and the locally generated reference signal.

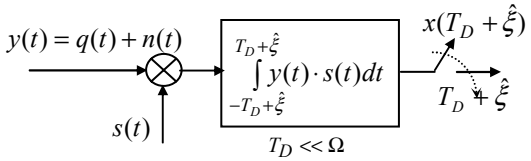

Figure 2: Illustration of correlator timing error detector. The input signal and the reference signal is multiplied and integrated over a period of $2T_D$ to obtain the timing error output.

If we impose the conditions that $q(t) = 0$ and $r(t) = 0$ for $|t| > T_D$, and $T_D << \Omega$, we can let $2T_D$ be the duration of the finite integration performed by the timing detector. This allows us to express the open-loop output of the timing detector by (5), where for simplicity, we have let $\theta = 0$, assuming the TLL is already in the tracking mode.

$$x_k = x(T_D + k\Omega + \hat{\xi}) = K_D \int_{-T_D+k\Omega+\hat{\xi}}^{T_D+k\Omega+\hat{\xi}} y(t) A_r r(t-\hat{\xi})dt \qquad (5)$$
$$= K_D g(T_D + k\Omega - \varepsilon_k) + K_D n'(T_D + k\Omega + \hat{\xi})$$

In (5), K_D is the detector gain and

$$g(T_D + k\Omega - \varepsilon_k) = A_s A_r \int_{-T_D+k\Omega-\varepsilon_k}^{T_D+k\Omega-\varepsilon_k} q(t) r(t+\varepsilon_k)dt, \qquad (6)$$

$$n_k' = n'(T_D + k\Omega + \hat{\xi}) = A_r \int_{-T_D+k\Omega+\hat{\xi}}^{T_D+k\Omega+\hat{\xi}} n(t) r(t-\hat{\xi})dt. \qquad (7)$$

The noise sample n_k' is a random variable obtained nominally at time interval $k\Omega$. Its auto-correlation function is not a function of timing error. It is not surprising since noise variables separated Ω seconds or more apart are not correlated for sufficient large Ω. This condition is easily satisfied for UWB systems where the impulse train typically has low duty cycle. A general timing detector model, operating at nominal pulse-repetition rate, which is similar to the general phase detector model of [1], can be written as:

$$x_k = K_D g(T_D + k\Omega - \varepsilon_k) + K_D n_k'. \qquad (8)$$

The simplicity in form of (5), (6) and (7) can be attributed to the fact that we have assumed a low duty cycle system such that there is no overlap of adjacent pulses and the channel is impaired only by AWGN. In addition, if the UWB monocycle is sufficiently ultra-wideband and assuming there are a finite number of multipaths whose strength does not diminish in the resolution process, we will be able to resolve all multiple components. Thus there will be minimal overlap of multipath pulses. Without lost of generality, we consider only one period of the correlation and drop the subscript *k* from ε. Thus the characteristic function of the TLL is:

$$g(\varepsilon) = A_s A_r \int_{-\infty}^{\infty} q(t) r(t+\varepsilon)dt. \qquad (9)$$

During tracking, ε fluctuates about the stable equilibrium point at $\varepsilon = 0$. We can then linearize the TLL by approximating $g(\varepsilon)$ around $\varepsilon = 0$ by $g(\varepsilon) = \varepsilon g'(0)$ where $g'(\varepsilon) = dg(\varepsilon)/d\varepsilon$.

III. Optimal Reference Waveform

After establishing the behavior of the timing detector, we devised the equivalent error-tracking TLL linear model as shown in Fig. 3. The digital loop filter is denoted as *D(z)* and a description of it can be found in [9].

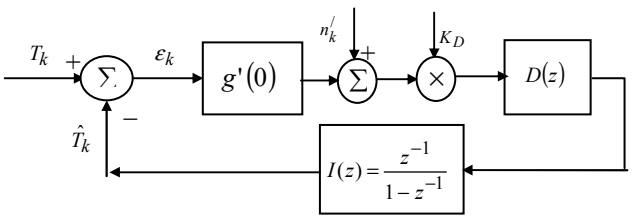

Figure 3: Equivalent timing model for the tracking of UWB impulses.

If $Z(u_k)$ is the Z-transform of u_k, from Fig. 3, we have

$$\frac{Z(\varepsilon_k)}{Z(n_k')} = \frac{-K_D D(z)}{1/I(z) + K_D g'(0) D(z)}. \qquad (10)$$

The parameter K_D is commonly chosen to make the effective gain of the TLL operating in the linear region equal to 1. This requires $K_D = 1/g'(0)$. After closing the loop, the timing error variance, assuming $D(z)$ and $I(z)$ are fixed, is proportional to

$$\sigma_\varepsilon^2 = \mathrm{E}\{\varepsilon^2\} \propto \frac{N_0}{2A_s^2} \cdot \gamma \tag{11}$$

and

$$\gamma = \frac{\int_{-\infty}^{\infty} r^2(t)dt}{\left[\frac{d}{d\varepsilon}\int_{-\infty}^{\infty} q(t)r(t+\varepsilon)dt\Big|_{\varepsilon=0}\right]^2}. \tag{12}$$

The ratio γ contains all dependence of σ_ε^2 on $q(t)$ and $r(t)$.

Clearly, to minimize the effect of the input noise on the timing error variance while having constant signal and noise ratio, the task is to minimize γ. The denominator of γ can be written as:

$$\frac{d}{d\varepsilon}\int_{-\infty}^{\infty} q(t)r(t+\varepsilon)dt\Big|_{\varepsilon=0} = \int_{-\infty}^{\infty} F_q(f)\,\overline{j2\pi f F_r(f)}\,df \tag{13}$$

where $\overline{R(f)}$ is the conjugate of $R(f)$ and $F_r(f)$ the Fourier transform of $r(t)$. Let $\langle x, y\rangle = \int x(t)\cdot\overline{y(t)}dt$ be the usual inner product space in $L_2(-\infty,\infty)$. We denote a bounded linear operator on a Hilbert space as K and its adjoint K^* such that $<x, K^* y> = <Kx, y>$. Here, these linear operators on $F_r(f)$ can be written as:

$$\begin{cases} K: F_x(f) \to \overline{j2\pi f}\, F_x(f) \\ K^*: F_x(f) \to j2\pi f\, F_x(f) \end{cases} \tag{14}$$

K^* is shown to be unique in [10]. Applying the Schwartz inequality to (12), we obtain

$$\begin{aligned} \gamma &= \frac{\|F_r(f)\|^2}{\langle F_q(f), K^* F_r(f)\rangle^2} = \frac{\|F_r(f)\|^2}{\langle KF_q(f), F_r(f)\rangle^2} \\ &\geq \frac{\|F_r(f)\|^2}{\|KF_q(f)\|^2\|F_r(f)\|^2} = \frac{1}{\|KF_q(f)\|^2} \end{aligned} \tag{15}$$

Equality occurs when $F_r(f) = -\beta j2\pi f F_q(f)$ or $r(t) = -\beta q'(t)$. Thus the optimal reference signal is the time derivative of the received monocycle waveform.

This result has been arrived at using different techniques in different contexts. For example, [13] presented a similar result, which also uses linear theory and the Schwartz inequality, for despreading chip waveform design in an early-late code tracking loop and the formulation includes effects of early-late spacing. We should further add that multiplying the received signal with the first derivative of the receiver generated replica of the transmitted signal has already being known as the maximum likelihood (ML) timing/phase estimator in AWGN as discussed in [12]. Our derivation can be viewed as a special case of [14] and is included here for completeness. The Cramer-Rao bound on the timing error variance for the ML detector as derived in [1], [2] and [15] is:

$$\mathrm{E}\{\varepsilon^2\} \geq N_o / 2E_r\varpi^2 \tag{16}$$

where E_r is the received signal energy per pulse and $\varpi^2 = \int_{-\infty}^{\infty} \omega^2 |F_q(\omega)|^2 d\omega / 2\pi$.

IV. UWB Monocycle Model

We model the received UWB monocycle pulse as the n^{th} order ($n>0$) derivative $w_n(t)$ of the Gaussian function. The time domain and frequency domain representations are given by (17) and (18) respectively. Here σ is a scaling factor that has the unit of time (e.g., seconds) and $p = 1/2\sigma^2$, (2n-1)!!=(2n-1)(2n-3)…...3.1.

$$w_n(t) = (-1)^{\lfloor (3n+1)/2 \rfloor} n!\,\pi^{-1/4} e^{-pt^2} \times \sum_{k=0}^{\lfloor n/2 \rfloor} \frac{(-1)^k 2^{n+1/4-2k} p^{n/2+1/4-k} t^{n-2k}}{(n-2k)!k!\sqrt{(2n-1)!!}} \tag{17}$$

$$W_n(f) = \frac{(-1)^n i^{n^2} (2\pi)^{n+\frac{1}{4}} p^{-\left(\frac{n}{2}+\frac{1}{4}\right)}}{\sqrt{(2n-1)!!}} f^n e^{-\pi^2 f^2/p}. \tag{18}$$

The monocycle waveform (17) has the following properties: (a) For $n = even$, the maximum amplitude is at $t=0$ and positive. (b) For $n=odd$, the slope at $t=0$ is positive. (c) The monocycle has unit energy, i.e., $\int_{-\infty}^{\infty} w_n^2(t)dt = 1$, and satisfies $w(t) \approx 0$ for $|t| \geq T_D$. The proposed model is a function of 3 parameters, the peak amplitude A_s, the order of the derivative n and a scaling factor σ. Increasing the derivative order of the monocycle waveform has the effect of shifting the spectrum to occupy a higher frequency range as shown in Fig. 4. Maintaining the same energy per pulse, a larger scaling factor stretches the monocycle pulse wider in time and thus a more gradual rise of the main lobe of the waveform. The amplitude also has a role to play in defining the final shape of the monocycle waveform besides directly affecting the SNR.

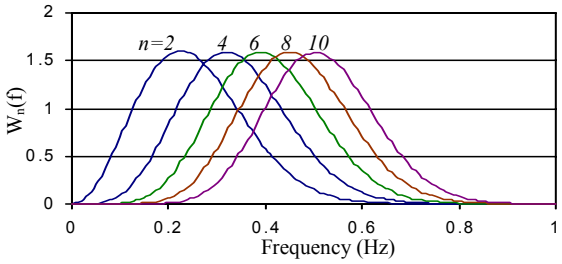

Figure 4: Fourier transform of $w_n(t)$ pulse with σ=1.

In Fig. 5, we fit $w_4(t)$ to an empirically measured UWB impulse (with the amplitude at $t=0$ normalized to 1) obtained inside an anechoic chamber. The antenna used is a diamond dipole antenna. In Fig. 6, the same $w_4(t)$ is fitted to UWB signals measured in an indoor office environment.

We observe that the model as given by (17) fits a possible class of UWB impulses radiated from dipole antenna. Such a UWB monocycle waveform, which is even symmetric about its peak with side lobes on each side of a main lobe is said to be the typical time-domain response of a continuously loaded dipole [6]. Similar monocycle waveforms, possibly of order higher than 4, have also been used in [7].

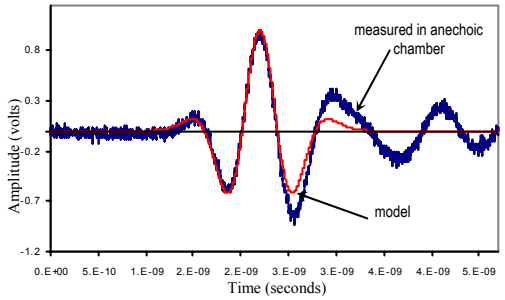

Figure 5: Comparison between experimentally measured and the analytic UWB monopulse. The signal is sampled at 2.5 pico-secs and σ =100 sample points or 2.5 x 10^{-10} seconds.

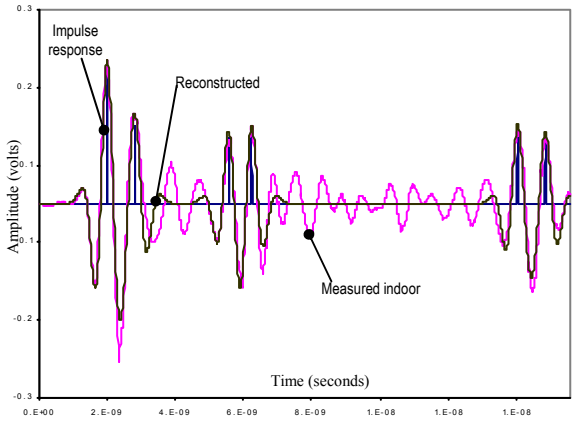

Figure 6: Antennas are spaced 2.5m apart with a clear Line of Sight. The reconstructed signal is obtained by convolution of the estimated channel impulse response with the UWB monocycle model given by (17) using σ=2.5391x10^{-10} secs. We have arbitrarily chosen the six strongest paths to form the channel impulse response.

V. TLL PERFORMANCE

If $q(t)=w_n(t)$ and $r(t)=w_m(t)$, from (12) and (17), we obtain the gradient of the slope at $\varepsilon=0$ as in (19). It is noted here that a larger gradient corresponds to a larger pull-in force for the TLL to achieve lock.

$$\frac{d}{d\varepsilon}\int_{-\infty}^{\infty} w_n(t)w_m(t+\varepsilon)dt\Big|_{\varepsilon=0} = \begin{cases} (-1)^n\sqrt{p}\,\dfrac{(n+m)!!}{\sqrt{(2n-1)!!(2m-1)!!}} & \text{if } n+m+1=\text{even} \\ 0 & \text{otherwise} \end{cases} \quad (19)$$

It can be shown that in the optimal case when $m=n+1$, we have for n even:

$$\varpi^2 = \left(\frac{d}{d\varepsilon}\int_{-\infty}^{\infty} w_n(t)w_m(t+\varepsilon)dt\Big|_{\varepsilon=0}\right)^2 = (2n+1)p \quad (20)$$

In table 1, we tabulated the ratio γ for various values of n and m. It indicates that a higher order Gaussian monocycle is desirable if the objective is to reduce the effect of AWGN at the input of the TLL by reducing the timing error variance. The improvement when raising the order from *(n=2,m=3)* to *(n=10,m=11)* is as high as 6.23dB. It seems that a higher order Gaussian monocycle has a main lobe that rises faster than a lower order pulse which contributes to this gain.

Table 1: The ratio γ for various values of n and m ($\begin{matrix} q(t)=w_n(t) \\ r(t)=w_m(t) \end{matrix}$)

	m=2	3	4	5	6
N=2		$1/(5p)$	-	$9/(35p)$	
3	$0.20/p$	-	$1/(7p)$	-	$11/(63p)$
4	-	$\approx 0.14/p$	-	$1/(9p)$	-
5	$\approx 0.26/p$	-	$\approx 0.11/p$	-	$1/(11p)$
6	-	$\approx 0.17/p$	-	$\approx 0.09/p$	-
7	$\approx 0.45/p$	-	$\approx 0.13/p$	-	$\approx 0.08/p$
8	-	$\approx 0.28/p$	-	$\approx 0.10/p$	-

The next reference signal function to be analyzed is the Hilbert transform of $w_n(t)$ (denoted $\tilde{w}_n(t)$). The general formulae for $\tilde{w}_n(t)$ is omitted as its complexity does not allow tractable mathematical analysis. Instead we present only $\tilde{w}_4(t)$ which is obtained with the aid of [4] and [5].

$$\tilde{w}_4(t) = \frac{2^{11/4}\pi^{3/4}p^{1/4}}{\sqrt{105}}\left\{\left(\sqrt{2p}\left(5t-2pt^3\right)\right)+ \sqrt{\pi/2}\left(4p^2t^4-12t^2p+3\right)\Im\left(\Omega\left(-it\sqrt{p}\right)\right)\right\} \quad (21)$$

where $\Omega(z)\equiv e^{-z^2}\,erfc(-iz)$ [6]. Here $\Im(\circ)$ is used to denote the imaginary part of a complex function.

If $q(t)=w_n(t)$ and $r(t)=\tilde{w}_n(t)$, we obtained numerically the ratio γ and tabulated it in Table 2. There is no significant difference between using the next higher order derivative (which is the optimal) or the Hilbert transform of the received waveform as the reference signal.

Reference [16] analyzed timing jitter via specific system simulation employing a monocycle waveform similar to the *n*=2 Gaussian derivative function and a conventional early-late gate tracking loop. In such early-late loops, the received signal is multiplied by early and late reference signals (or their difference) typically matched to the transmitted signal pulse shape. We will not reproduce the results of [16] here because we have shown in Section III that the ML optimal reference waveform is the derivative of the received signal. Instead, we present our next result when the reference signal $r(t)$ is of the form:

$$w_\tau(t) = \begin{cases} 1/\sqrt{2\tau} & 0<t<\tau \\ -1/\sqrt{2\tau} & -\tau<t<0 \\ 0 & \text{otherwise} \end{cases} \quad (22)$$

Equation (22) represents a reference signal waveform that can be implemented easily. The slope at $\varepsilon = 0$ when the received signal is $w_n(t)$ and n even is:

$$\frac{d}{d\varepsilon}\int_{-\infty}^{\infty} w_n(t)w_r(t+\varepsilon)dt\Big|_{\varepsilon=0} = \frac{i^{n^2+n}\,2^{n+1/4}\,p^{n/2-3/4}\,\pi^{-1/4}(n-1)!}{\sqrt{(2n-1)!!}}\times \left\{\sum_{k=0}^{\left\lfloor\frac{n-1}{2}\right\rfloor}\frac{(-1)^k 2^{-2k}p^{-k}}{(n-1-2k)!k!}\left(e^{-\tau^2 p}\tau^{n-2k}[(n-2k-1)\tau^{-2}-2p]\right)- \frac{(-1)^k 2^{-2k}p^{-k}}{k!}\Big|_{k=\left\lfloor\frac{n-1}{2}\right\rfloor}\right\} \quad (23)$$

In Fig. 7, we plotted (23) as a function of τ for $n = 2,4,6,8$ and 10. As expected, as τ increases, the slope approaches a non-zero limiting values. And there is an optimal $\tau = \tau_{\max}$ that maximizes the gradient. For all cases considered, through careful simulation, $\tau_{\max}$ is close to the width from the peak at $t = 0$ to the first negative peak of $w_n(t)$ as illustrated in Fig. 8. The ratio γ when $\tau = \tau_{\max}$ is tabulated in Table 2. As the order n increases, the timing error variance with $r(t) = w_r(t)$ degrades compared to the optimal $r(t) = w_{n+1}(t)$. At $n = 2$, the difference is about 0.98 dB while at $n = 10$, the difference is as high as 2.5 dB. At $\tau = 16\sigma$, $\sigma = 1$, γ is about 10.406 for all n in Fig. 7, this is about 17.9 dB away from the optimal when $n = 10$.

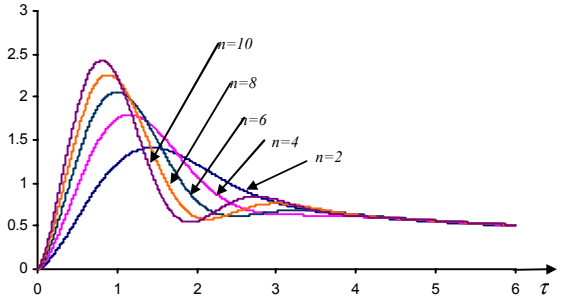

Figure 7: Gradient of the S-curve at $\varepsilon = 0$ when $q(t) = w_n(t)$ and $r(t) = w_r(t)$ for various n as a function of τ. We have fix $\sigma = 1$.

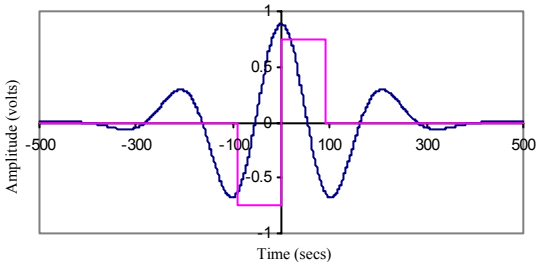

Figure 8: Illustration of $w_n(t)$ and $w_r(t)$ when $\tau = \tau_{\max}$. Here $n = 8$, $\sigma = 1$, $A_s = A_r = 1$ and the sampling rate is 0.01 secs.

Table 2: Comparison of γ for higher order Gaussian derivative and Hilbert transform reference signals

n	$\gamma(n, n+1)$ $\sigma^2 = 1$	$\gamma(n, Hilbert)$ $\sigma^2 = 1$	$\gamma(n, w_r(t))$ $\sigma^2 = 1, \tau = \tau_{\max}$
2	0.4000	0.4418	0.5021
4	0.2222	0.2349	0.3100
6	0.1538	0.1599	0.2358
8	0.1176	0.1212	0.1957
10	0.0952	0.0975	0.1701

We continue with our analysis of the TLL by examining its phase-plane plot. The phase plane plot is obtained by simulating the TLL shown in Fig. 1. The digital loop filter is of the form $D(z) = G_1 + G_2 z/(z-1)$ with G_1=*0.28* and G_2=*0.06*. Thus we have a 2nd order loop which is able to handle mismatch between the transmitter and receiver pulse-repetition-rate.

In Fig. 9 and 10, an example of the TLL phase-plane for two different pairs of *q(t)* and *r(t)* are shown. In both figures, the same *D(z)* is utilized in the TLL. When *(n=4,m=5),* the TLL cannot acquire lock for $|\theta|$ as small as 0.2σ. After we reduce the order to *(n=2,m=3),* lock acquisition is still possible for $|\theta| = 0.3\sigma$. It illustrates that lower order n and m can acquire lock for a larger range of mismatch in pulse repetition rate θ.

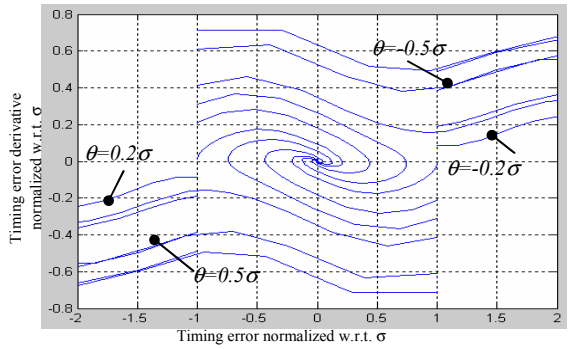

Figure 9: Phase-plane $(d\varepsilon/dt)$ *vs* ε for a second order loop. Here $q(t) = w_4(t)$ and $r(t) = w_5(t)$.

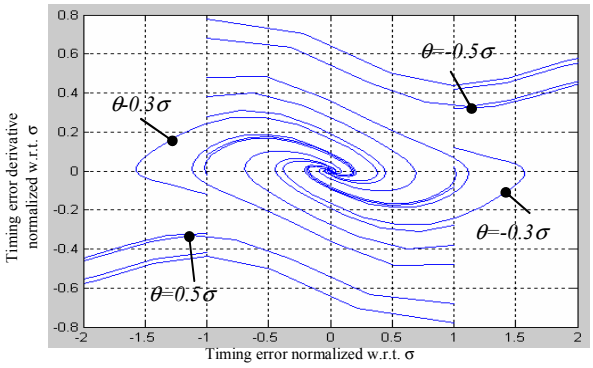

Figure 10: Phase-plane $(d\varepsilon/dt)$ *vs* ε for a second order loop. Here $q(t) = w_2(t)$ and $r(t) = w_3(t)$.

VI. MATCH FILTER & AGC PRE-PROCESSING

There are three main issues that need to be addressed before the tracking loop described in previous sections can be effective. Firstly, the received UWB impulse may not be even symmetric about its peak and may have a more complicated form then that prescribed in our model for a realistic multipath channel. This will result in a fixed bias in the timing detector output that can vary according to the channel. Secondly, unlike baseband communication, UWB impulse transceivers use pulses of nanosecond width with very low duty cycle. As a result, the lock range is small. Thus, we may need an initial estimate of the time-of-arrival of the UWB impulses at the receiver. Lastly, (9) suggests that the loop gain is a function of the signal amplitude A_s. This is undesirable. Generally, the receiver is required to maintain essentially a constant loop gain during operation in order to maintain a stable closed-loop time-error tracking system. We thus require some form of automatic gain control (AGC) circuits to provide amplitude and thus gain stability [2][8].

To mitigate the second and third constraints, we suggest placing a peak searching matched filter, with modification from its conventional form to provide an initial estimate of A_s, before the TLL to generate an estimate as shown in Fig.11.

The peak searching matched filter works by passing the received signal through a matched filter followed by a zero-crossing detector as shown in Fig. 11. As stated in [3], the output of the matched filter is first differentiated. If the matched-filter output is above a detection threshold, indicating the presence of a valid signal, the zero crossing of the derivative signal will trigger a timing marker indicating the occurrence of a peak correlation between the reference and input signal. The timing marker will also trigger a circuit that samples the peak of the correlation output to provide an initial estimation $\hat{A}_s$. It is said that the SNR at the output of the matched filter must be large (at least large enough for reliable detection) to prevent gross errors caused by noise peaks not associated with a signal.

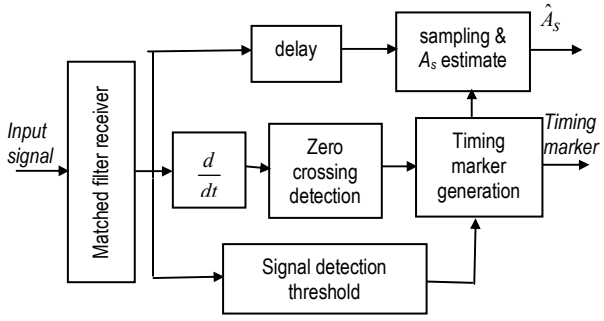

Figure 11: A modified "linear filter (slope-reversal) estimator" [3] to estimate the time delay and amplitude of received UWB monocycle.

VII. CONCLUSIONS

We have not analyzed the effect of the one-sided loop bandwidth on the performance of the TLL. In narrowband communications, it is usually assumed that the received signal timing process fluctuates very slowly with respect to the channel symbol period to justify the use of a small loop bandwidth to reduce the effect of noise on the timing error. However, it is not clear whether the same assumption of slow fluctuations is applicable for UWB systems.

The release of the FCC First R&O on UWB transmissions opens up a very large bandwidth for the possible use of UWB devices transmitting impulses. As a result, there is considerable freedom in the choice of the signal waveform to exploit this ultra-wide bandwidth for novel applications. The proposed model, though ideal, is more comprehensive than the 2nd order model currently used in the literature, and at the same time, provides more design parameters to the engineer designing an UWB device. For example, from our analysis, we may first choose a lower order monocycle pulse for the purpose of acquiring lock. After this, we can change to a higher order monocycle pulse to reduce the variance of the timing jitter due to additive noise in the input.

ACKNOWLEDGEMENT

We wish to thank the anonymous reviewers for their helpful comments.

REFERENCES

[1] Heinrich Meyr, Marc Moeneclaey and Stefan A. Fechtel, *Digital Communication Receivers – Synchronization, Channel Estimation, and Signal Processing*, Wiley, 1998.

[2] Merrill I. Skolnik, *Introduction to Radar Systems*, 2nd Edition, McGraw-Hill, Chapters 10 and 11, 1980.

[3] Eli Brookner (Editor), *Radar Technology*, Artech House, Chapters 6 and 11, 1978.

[4] I. S. Gradshteyn and I. M. Ryzhik, *Table of Integrals, Series, and Products*, equation 3.462, 5th edition, Academic Press.

[5] Milton Abramowitz and Irene A. Stegun, *Handbook of Mathematical Functions with Formulas, Graphs, and Mathematical Tables*, National Bureau of Standards (US Department of Commerce)-Applied Mathematics Series 55, 10th printing, Chapter 7, eqn 7.1.3, Dec 1972.

[6] D. J. Daniels, *Surface Penetrating Radar*, The Institute of Electrical Engineers, Chapter 4.2, 1996.

[7] Robert Fontana et. al., "*Recent advances in Ultra Wideband Communications Systems*", IEEE Conference on Ultra Wideband Systems and Technologies, 2002.

[8] Heinrich Meyr and Gerd Ascheid, *Synchronization in Digital Communications – Volume 1, Phase-, Frequency-Locked Loops, and Amplitude Control*, Wiley 1990.

[9] William C. Lindsey and Chak Ming Chie, "A Survey of Digital Phase-Locked Loops", Proceedings of the IEEE, vol. 69, No.4, April 1981.

[10] Arch W. Naylor and George R. Sell, *Linear Operator Theory in Engineering and Science*, Springer-Verlag 2000, page 352 to 360.

[11] Lindsey, W.C., Synchronization Systems in Communication and Control, Prentice Hall, 1972, Chapter 2.

[12] R. L. Peterson, R. E. Ziener and D. E. Broth, Introduction to Spread Spectrum Communications, Prentice Hall 1995, Chapters 4 and 5.

[13] Xiaofu Wu, Cong Ling and Haige Xiang, "Despreading Chip Waveform Design for coherent delay-locked tracking in DS/SS systems", ICC 2002, page 631-635.

[14] R. Sampaio-Neto and R. A. Scholtz, "Precorrelation Filter Design for Spread-Spectrum Code Tracking I Interferene", IEEE JSAC, vol. SAC-3, No. 5, Sept 85.

[15] Harry L. Van Trees, *Detection, Estimation, and Modulation Theory: Part III – Radar-Sonar Signal Processing and Gaussian Signals in Noise*, Chapters 6.2, 9.2, 10.1 and 10.2, Wiley 1971.

[16] W. M. Lovelace and J. K. Townsend, "The Effects of Timing Jitter and Tracking on the performance of Impulse Radio", IEEE JSAC, vol 20, No. 9, Dec 2002.